

MeshArt: Generating Articulated Meshes with Structure-guided Transformers

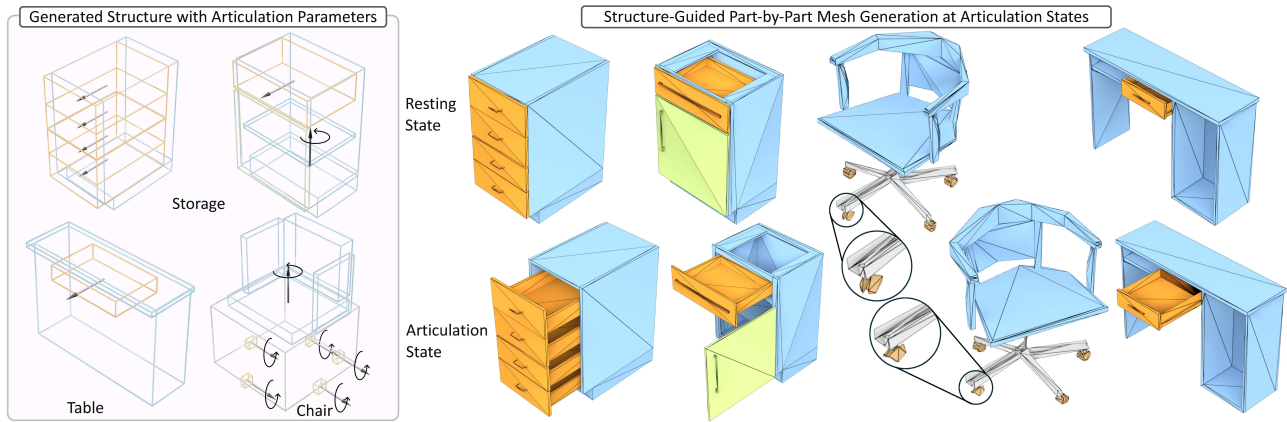
Daoyi Gao¹Yawar Siddiqui^{1,2}Lei Li¹Angela Dai^{1,2}¹Technical University of Munich²Meta

Figure 1. MeshArt creates articulated 3D objects hierarchically, part-by-part with transformers by first generating high-level object structures endowed with articulations (**left**) and then predicting triangle mesh faces for each part (**right**) with structure and local connectivity guidance. Our mesh generations have clean and compact triangulations and can be animated at different articulation states.

Abstract

Articulated 3D object generation is fundamental for creating realistic, functional, and interactable virtual assets which are not simply static. We introduce MeshArt, a hierarchical transformer-based approach to generate articulated 3D meshes with clean, compact geometry, reminiscent of human-crafted 3D models. We approach articulated mesh generation in a part-by-part fashion across two stages. First, we generate a high-level articulation-aware object structure; then, based on this structural information, we synthesize each part’s mesh faces. Key to our approach is modeling both articulation structures and part meshes as sequences of quantized triangle embeddings, leading to a unified hierarchical framework with transformers for autoregressive generation. Object part structures are first generated as their bounding primitives and articulation modes; a second transformer, guided by these articulation structures, then generates each part’s mesh triangles. To ensure coherency among generated parts, we introduce structure-guided conditioning that also incorporates local part mesh connectivity. MeshArt shows significant improvements over state of the art, with 57.1% improvement in structure coverage and a 209-point improvement in mesh generation FID.

1. Introduction

Articulated objects are ubiquitous in real-world environments – for instance, cabinet doors are openable, office chairs typically swivel, car wheels and doors rotate and move. These articulations are generally tied to the core functionality of these objects (e.g., storage for cabinets, ease of movement for chairs, movement of cars), and are thus key to representing realistic, interactable objects. Such objects are already widely represented in computer graphics applications as triangle meshes, carefully crafted by skilled 3D artists. This enables high visual quality while maintaining a compact representation that readily supports the articulated motion of various object parts.

Recent advances in generative modeling for vision and graphics have produced remarkable progress in generating static 3D objects [2, 4, 27–29, 40] as well as complex static 3D scenes [19, 26, 37], leveraging various 3D representations, from voxels and point clouds to neural fields and even 3D meshes. However, generating articulated objects with dynamic, functional parts remains an underexplored challenge. The primary difficulties lie in not only modeling possible functional part motions but also generating clean and compact part geometries that respect the articulation structures. In particular, generating articulated objects as triangle meshes enables natural support of changing topological structure (e.g., open vs. closed doors in a

shelf) while maintaining a compact representation similar to human-crafted objects. Besides, current 3D datasets with object part and articulation joint annotations remain relatively limited in quantity for data-driven learning.

To address these challenges, we introduce MeshArt¹, a hierarchical transformer-based model that generates articulated 3D meshes with sharp details and an efficient triangle mesh representation, resembling the compactness of artist-created 3D models. Our key insight is to decompose articulated meshes into high-level object structures and low-level part geometries: high-level structures are represented by part bounding primitives endowed with articulation properties, while part geometries are generated based on both articulation structures and local mesh connectivity. To enable effective training of MeshArt, we enhance PartNet [21], the largest 3D object dataset with part labels, by adding articulation joint annotations to the table, chair, and storage categories, increasing the number of articulated objects 6× compared to existing articulation datasets [6, 38].

Our approach leverages a direct sequence generation approach with transformers to synthesize articulated objects hierarchically, part by part. We first predict the object structure as a sequence of part bounding boxes, where each box encodes part semantics, latent geometric features, and articulation properties. Using the predicted structure, we then generate the mesh geometry for each part as a sequence of triangles, conditioned on the structure and local connectivity from previously generated parts. To unify this hierarchical generation process, we also parameterize part bounding boxes as triangle meshes; this unified representation enables more effective generation of coherent articulated meshes.

At the object structure level, we learn a vocabulary of object structures by encoding triangulated part bounding boxes into quantized triangle embeddings, and then train a decoder-only transformer to autoregressively predict a triangle sequence representing the part bounding primitives. At the part geometry level, we learn a separate codebook that encodes both part mesh triangles and their likelihood of serving as junctions between parts. We then train another transformer to generate the triangle sequence for each part mesh, conditioned on the object structure embeddings and junction faces from neighboring parts, ensuring smooth transitions between parts. Experiments across three categories of our articulated PartNet dataset demonstrate that our method significantly improves both the diversity of articulation structures and the quality of generated 3D meshes compared to state-of-the-art methods, achieving an average improvement of 57.1% in structure coverage and a 209-point improvement in mesh generation FID scores.

In summary, our contributions are:

- We propose MeshArt, a novel hierarchical approach for generating articulated 3D objects, part by part to create

compact triangle meshes. Our approach unifies coarse articulation-aware structure generation with structure-guided part mesh generation, treating both as triangle sequence prediction tasks.

- We introduce a conditioning mechanism that integrates structure and local geometry connections to ensure smooth transitions during part-by-part mesh generation.
- We augment PartNet with joint annotations on 3 major categories, expanding the articulated object dataset by over 6 times.

2. Related Work

Mesh Generation. Several methods have been proposed to directly generate mesh representation, due to their compact nature more similar to human-created 3D models. Earlier approaches such as Scan2Mesh [3] proposed to generate mesh structures as graphs, but were limited to generation of small meshes with very limited number of vertices. PolyGen [22] proposed to employ two separate autoregressive transformers to learn the distributions of vertices and faces independently. Similarly, Polydiff [1] uses a diffusion model to generate triangle soups to construct meshes. MeshGPT [28] instead tokenizes mesh representations with a graph neural network (GNN)-based encoder and learns mesh tokens using a GPT-style transformer. PivotMesh [33] enhances such generation by guiding the process with pivot vertices that define the coarse shape of an object.

Despite these advancements, the functionality of the generated assets is often overlooked, as these methods all focus on static mesh generation. In contrast, our approach disentangles structural part semantics from geometry, employing an autoregressive model to facilitate the generation of functional articulated objects.

Structured Object Generation. Structure-aware generative models for 3D objects have focused on modeling object parts and their relationships. SAGNet [36] uses a VAE to encode part geometry and pairwise relations into a latent space, which is then decoded to generate coherent objects. GRASS [13] models part structure hierarchies as binary trees based on symmetry hierarchies [32], utilizing a recursive autoencoder to capture both parts and their geometric properties. StructureNet [20] extends this idea by representing objects as n-ary graphs, enabling the generation of more complex structures.

SDM-NET [5] combines deformable mesh boxes to represent part geometry and a VAE to encode the global structure, producing more detailed part geometries. DSG-Net [39] disentangles part geometry from structure by learning separate latent spaces for each, allowing fine-grained control during generation.

While these methods effectively generate coherent 3D shapes with structural parts, they do not account for artic-

¹[daoyig.github.io/Mesh_Art/](https://github.com/daoyig/Mesh_Art/)

ulation. In contrast, we encode articulation directly within the structural generation of triangle meshes, enabling the creation of compact, functional meshes with articulated properties.

Articulated Object Modeling. Recent advancements in articulated 3D object modeling have focused on reconstructing or generating objects with geometric and motion properties. Ditto [10] reconstructs articulated objects from point clouds as implicit representations, capturing geometric occupancy, part types, and joint parameters. Similarly, [9] and [16] reconstruct articulated objects as implicit neural fields from stereo RGB and point cloud videos, respectively. PARIS [14] disentangles static and movable parts from two observations at different articulation states, predicting both geometry and motion parameters. Building on this, [34] introduces explicit point-level correspondence between reconstructed shapes in two states, enabling the modeling of more complex articulated objects.

NAP [12] introduces the unconditional generation of articulated objects by modeling articulation parameters with geometry using an articulation tree. The final geometry is decoded either via an implicit field decoder or through part retrieval. CAGE [15] employs diffusion to generate articulation abstractions, relying on part retrieval for final object geometry. However, this part retrieval and assembly approach [30, 35, 41] can introduce inconsistencies in part geometry and overall shape structure. In contrast, our MeshArt generates both structure and geometry cohesively in a sharp, unified triangle mesh representation, enhancing the efficiency and robustness of articulated object modeling.

3. Method

Our goal is to generate articulated 3D objects in a compact triangle mesh representation with sharp geometric details. We formulate articulated mesh generation in a hierarchical, part-by-part fashion and propose MeshArt, a transformer-based approach that generates both part-level object structures and part mesh geometry as sequences of triangles.

To capture high-level object structures (Sec. 3.1), we decompose a 3D object into functional parts $\{\mathcal{P}^i\}$ and represent the object structure as $\mathcal{S} = \{s^i\}$. Each s^i encodes the bounding box, articulation properties, part semantics, and latent geometry features of part \mathcal{P}^i . This part-level abstraction enables efficient joint modeling of parts and articulation modes, providing global guidance for articulated mesh generation. To formulate structure generation as a sequence prediction task, we represent each part’s bounding box as a triangle mesh and learn a structure codebook \mathcal{C}_s to encode \mathcal{S} as a sequence of quantized triangle embeddings. A structure transformer Φ_s is trained to predict the next embedding index in this sequence. Once trained, Φ_s can be autoregressively sampled to generate articulated object structures.

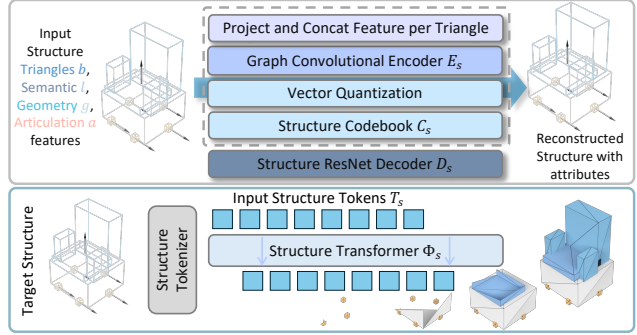


Figure 2. We model high-level object structures with articulations using a VQ-VAE for structure encoding (**top**) and a decoder-only transformer for autoregressive structure sequence generation (**bottom**). The encoder E_s first encodes triangulated part bounding boxes, along with semantics, coarse geometry, and articulation features, into a structure token sequence \mathcal{T}_s over a learned codebook \mathcal{C}_s . The structure transformer Φ_s then learns to predict the next token in \mathcal{T}_s , which is subsequently decoded by the decoder D_s to generate the object structure.

Next, we generate part geometry for \mathcal{P}^i as a sequence of mesh triangles, guided by the global object structure \mathcal{S} (Sec. 3.2). To further capture local geometry and connectivity between parts, we encode the mesh triangles of \mathcal{P}^i , along with their likelihood of being junction faces connecting different parts, as a quantized embedding sequence over a separately learned geometry codebook \mathcal{C}_g . This junction injection ensures smooth transitions between adjacent parts. A geometry transformer Φ_g then predicts the next triangle face embedding index, conditioned on \mathcal{S} and junction embeddings from neighboring parts. Finally, we decode the generated embeddings into a clean, compact part mesh.

3.1. Articulation-Aware Structure Generation

For an articulated object with functional parts $\{\mathcal{P}^i\}$, we represent its high-level structure as $\mathcal{S} = \{s^i\}$, capturing each part’s spatial location, articulation motion, semantic label, and coarse geometry guidance. Encoding articulation at the structure level abstracts away part geometry details, enabling efficient modeling of shared articulation modes across objects. Articulation modeling requires distinguishing between various articulated and static parts, and defining articulation properties, including joint types, locations, and orientations, as detailed below.

Structure Parameterization. For each part \mathcal{P}^i , we encode its bounding box b^i , articulation properties a^i , semantic label l^i , and latent geometry g^i as

$$s^i = (b^i, a^i, l^i, g^i). \quad (1)$$

The *part bounding box* b^i is represented as an axis-aligned bounding box (AABB) in the object’s canonical resting state (*e.g.*, doors and drawers are closed). For efficient sequence modeling and generation, as well as effective

conditioning for the mesh surface generation, we represent these bounding boxes as triangle meshes.

Articulation properties $\mathbf{a}^i = (\mathbf{j}^i, \mathbf{f}^i, \mathbf{o}^i, \mathbf{p}^i)$ include joint type \mathbf{j}^i , existence \mathbf{f}^i , orientation \mathbf{o}^i , and location \mathbf{p}^i . Three joint types are considered: *fixed*, *revolute*, and *prismatic*. The joint orientation is represented as a 3D unit vector. Prismatic joint locations are canonicalized to the object’s origin. The range for revolute joints is set to 90° , and the range for prismatic joints is determined by the object’s base extent.

The *part semantic label* \mathbf{l}^i is encoded as a feature vector using the CLIP text encoder [25].

Learning Quantized Structure Embeddings. To facilitate autoregressive generation of articulated object structures with transformers, we encode the structure information \mathcal{S} as a sequence of quantized triangle embeddings, as shown in Fig. 2-top. We adopt a bottom-up sequence ordering [22, 28], arranging the N part bounding box meshes $\{\mathbf{b}^i\}$ as a sequence of triangles:

$$\mathcal{M}_s := (f_1^1, \dots, f_{12}^1, \dots, f_j^i, \dots, f_{12}^N), \quad (2)$$

where f_j^i denotes the j -th triangle face of the i -th part bounding box mesh. Bounding boxes are sorted from bottom to top based on their lowest face locations. For each box mesh, vertices are sorted from lowest to highest in z - y - x order (vertical axis z), and the 12 triangle faces are then ordered by their lowest vertex, the next lowest, and so on.

Similar to MeshGPT [28], we then train a Vector Quantized-Variational Autoencoder (VQ-VAE) [31]; instead of learning a codebook encoding mesh triangles, we learn a structure codebook \mathcal{C}_s encoding a triangle-based representation of the coarse structure. The structure encoder \mathbf{E}_s employs graph convolutions [7] by treating the triangles in \mathcal{M}_s as nodes. Structure features from \mathcal{S} are independently projected and then concatenated with positionally encoded triangle coordinates as input features. The structure encoder \mathbf{E}_s extracts an articulation-aware feature vector for each structure triangle as

$$\mathcal{Z}_s = (\mathbf{z}_1^1, \dots, \mathbf{z}_j^i, \dots, \mathbf{z}_{12}^N) = \mathbf{E}_s(\mathcal{M}_s, \mathcal{S}), \quad (3)$$

where \mathbf{z}_j^i denotes the feature vector for f_j^i .

At the bottleneck, a residual vector quantization (RQ) module [18] assigns D codes to each structure triangle f_j^i , based on the learned embedding \mathbf{z}_j^i and codebook \mathcal{C}_s , resulting in a structure token sequence \mathcal{T}_s as

$$\mathcal{T}_s = (t_1^1, \dots, t_j^i, \dots, t_{12}^N) = \text{RQ}(\mathcal{Z}_s; \mathcal{C}_s, D), \quad (4)$$

where t_j^i consists of D embedding indices. A 1D-ResNet [8] decoder \mathbf{D}_s then decodes the quantized face embedding sequence to reconstruct the structure \mathcal{S} .

During training, to supervise the reconstruction of \mathcal{S} , we apply a cross-entropy loss to predict the quantized locations

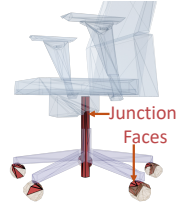
of bounding box triangles \mathbf{b}^i , joint type \mathbf{j}^i , joint existence \mathbf{f}^i , and joint location \mathbf{p}^i . Predicting locations as discretized coordinates helps stabilize training. We use an ℓ_2 loss for regressing the joint orientation \mathbf{o}^i , semantic feature \mathbf{l}^i , and geometry feature \mathbf{g}^i . We refer to the supplemental for more training details on the structure VQ-VAE.

Structure Generation with Transformers. Given the learned structure codebook \mathcal{C}_s , we use a GPT-style decoder-only transformer Φ_s to predict the structure token sequence \mathcal{T}_s , which is then decoded into an object structure \mathcal{S} by \mathbf{D}_s (Fig. 2-bottom). The structure transformer Φ_s is trained with a cross-entropy loss for next-token index prediction. Once trained, we use beam sampling to generate articulated structures unconditionally from Φ_s .

3.2. Structure-guided Part Mesh Generation

Next, we generate mesh triangles for each part \mathcal{P}^i , conditioned on the high-level object structure \mathcal{S} using a geometry transformer Φ_g over a separately learned triangle codebook \mathcal{C}_g , as illustrated in Fig. 3. Since we generate articulated object meshes part by part, we must ensure smooth connections to adjacent part meshes already generated. To address this, we introduce a junction face mechanism to guide triangle generation for a coherent 3D object mesh.

Junction faces are triangles that are spatially adjacent to different parts, providing crucial local geometry and connectivity cues for generating mesh triangles of a new part. For example, in the inset figure, junction faces of the chair wheels strongly indicate the chair base shape and connection points. We thus incorporate junction face information into the geometry codebook \mathcal{C}_g and condition the geometry transformer Φ_g additionally on these junction faces to ensure structural continuity, as detailed below.



Junction-aware Triangle Encoding. We first encode each part mesh \mathcal{P}^i as a sequence of quantized triangle embeddings using the geometry codebook \mathcal{C}_g (Fig. 3-left), similar to the structure embedding in Sec. 3.1.

Triangles in \mathcal{P}^i are sorted bottom-up in a sequence $\mathcal{M}_g^i = (f_1^i, f_2^i, \dots, f_{N_i}^i)$. A graph convolutional [7] geometry encoder \mathbf{E}_g extracts informative geometric features \mathcal{Z}_g^i for the triangles as: $\mathcal{Z}_g^i = \mathbf{E}_g(\mathcal{M}_g^i)$. An RQ module then quantizes these features, assigning D codes per triangle based on the learned codebook \mathcal{C}_g as $\mathcal{T}_g^i = \text{RQ}(\mathcal{Z}_g^i; \mathcal{C}_g, D)$.

We employ a 1D ResNet decoder with two prediction heads. One head reconstructs the triangle coordinates of \mathcal{P}^i from the quantized embeddings, supervised by a cross-entropy loss. The other head predicts the probability p_k^i for each face $f_k^i \in \mathcal{M}_g^i$ to be a junction face connecting to other parts, thereby injecting junction information into \mathcal{C}_g . To su-

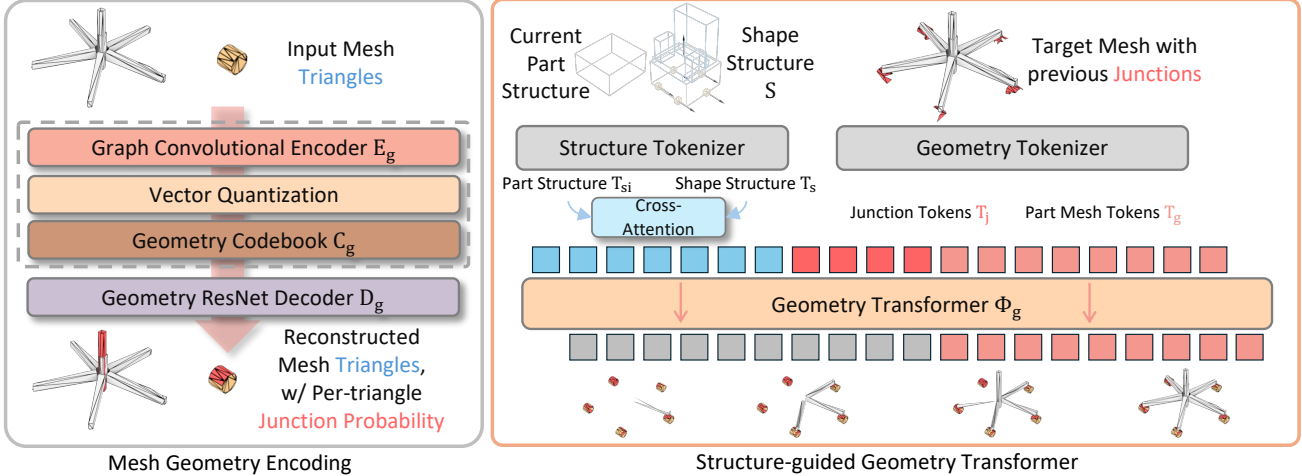


Figure 3. We generate mesh triangles for a 3D object part by part, guided by the high-level object structure \mathcal{S} and junction connections to previously generated part meshes. **Left:** The encoder \mathbf{E}_g encodes triangles of each part mesh into a sequence of quantized triangle embeddings \mathcal{T}_g , using a separately learned geometry codebook \mathcal{C}_g . The decoder \mathbf{D}_g then reconstructs the mesh triangles from \mathcal{T}_g and predicts a junction probability for each face connecting to other parts. **Right:** The geometry transformer is conditioned on the current part structure, the overall object structure \mathcal{T}_s , and junction face tokens to predict the triangle tokens \mathcal{T}_g for generating the current part mesh.

pervise junction predictions, we identify the ground-truth junction faces by calculating the distance between each triangle in \mathcal{P}^i and neighboring parts, labeling as junction faces if their distances fall below a predefined threshold.

Part Mesh Generation with Transformers. We train the geometry transformer Φ_g to predict the triangle token sequence \mathcal{T}_g^i , guided by the object structure \mathcal{S} and junction face tokens from neighboring parts (Fig. 3-right).

The input sequence for Φ_g is constructed by placing the structure and junction tokens at the beginning, followed by the triangle tokens \mathcal{T}_g^i . Concretely, for the current part mesh \mathcal{P}^i , its corresponding structure tokens $(t_1^i, \dots, t_{12}^i) \subset \mathcal{T}_s$ are extracted and cross-attended to the overall object structure \mathcal{T}_s , before being added to the start of the sequence. Next, we retrieve ground-truth junction faces from other parts and append their tokens to the sequence, prior to triangle tokens \mathcal{T}_g^i . These junction tokens inform smooth transitions and connectivity between neighboring parts.

The complete sequence is then fed into Φ_g , which has a stack of multi-head self-attention layers, to predict the next triangle token in the sequence. We apply a cross-entropy loss to the predicted triangle tokens \mathcal{T}_g^i , while the injected structure and junction tokens serve solely as conditioning.

Due to the varying length of the condition sequence, depending on the number of junction faces, standard index-based positional embeddings would result in inconsistent embeddings for the start token of the mesh sequence \mathcal{T}_g^i . We employ a flexible positional embedding scheme to address this: we fix the positional embeddings starting from \mathcal{T}_g^i , while applying a constant positional embedding vector for the preceding condition sequence.

3.3. Hierarchical Articulated Mesh Sampling

For articulated mesh generation at inference time, we first sample the structure transformer Φ_s unconditionally to generate an object structure sequence \mathcal{S} in an autoregressive manner. The structure decoder \mathbf{D}_s then decodes \mathcal{S} into part bounding boxes with associated articulation properties.

Next, for each part \mathcal{P}^i , we generate its mesh triangle sequence \mathcal{T}_g^i by sampling the geometry transformer Φ_g , conditioned on object structure \mathcal{S} and predicted junction faces from previously generated part meshes. Only junction faces that are spatially near the bounding box \mathbf{b}^i of \mathcal{P}^i are considered. The predicted triangle tokens \mathcal{T}_g^i are then decoded into mesh triangles by the geometry decoder \mathbf{D}_g . Finally, the object mesh is obtained by merging close vertices of the generated triangles. This articulated mesh can be transformed into different articulation states based on the structure-level joint predictions.

4. Articulated PartNet Dataset Annotations

Previous methods for generating articulated objects [12, 15] primarily relied on the PartNet-Mobility dataset [38], which comprises a small number of objects (c.f. Tab. 1) with limited diversity in articulated structures. We thus instead augment the PartNet dataset [21] across 3 major categories by annotating articulation information for functional parts such as cabinet doors, drawers, and wheels. As shown in Tab. 1, our annotations increase the number of articulated parts by more than $6\times$ compared to PartNet-Mobility.

To ensure accurate annotations of joint locations and orientations, we 1) manually corrected inconsistencies in mesh orientations and part groupings; 2) automatically annotated prismatic joints, aligning all joints to the object space ori-

Categories	Storage Furniture	Table	Chair
PartNet-Mobility [38]	346	101	81
Ours (Articulated PartNet)	1786	1454	372

Table 1. Our annotated articulated PartNet [21] significantly increases the number of articulated objects.

gin; 3) generated hypotheses for revolute joints and manually selected the most plausible options through an interactive interface; and 4) manually verified and adjusted joints based on renderings of articulated part motions. Overall, we dedicated over 150 hours to constructing this PartNet extension. We refer to the supplemental for further details.

5. Experiments

We present results using our annotated Articulated PartNet.

Implementation. To learn the structure and geometry codebooks, our RQ layer has a depth of 2, yielding $D = 6$ embeddings per face, each with dimension 192. For the triangle location prediction, both structure and geometry decoders predict face coordinates across 128 classes, resulting in a discretization of space to 128^3 possible values. The structure decoder also regresses the 768-dim part semantic features and 128-dim latent geometry features. For the structure transformer Φ_s , we use a GPT2-small model with a context window of 4608, and for the geometry transformer Φ_g , we use a GPT2-medium model of the same window length. We implemented our approach using PyTorch [23].

Training. During training, we employ augmentation techniques including random shifts and random scaling to enhance the training mesh diversity. Similar to MeshGPT [28], we apply planar decimation to augment the shapes. To ensure that a part mesh fits into the geometry transformer’s context window, we select the object parts with < 700 faces (post-decimation) for training.

We begin by training both the VQ-VAEs and transformer models across all 3 (chairs, tables, storage) categories and then fine-tune the transformers on each category individually. We use a 90/10 training/testing split for each category. The structure VQ-VAE is trained on one A6000 GPU for 3 days, and the geometry VQ-VAE is trained on one A100 for 2 days until convergence. Pretraining Φ_s takes 3 days on a single A100 GPU, followed by 1 day for fine-tuning on each category. Pretraining Φ_g takes ~ 4 days on four A100 GPUs, followed by 2 days per category for fine-tuning on a single A100. We use the ADAM optimizer [11] with a learning rate of 1×10^{-4} and a batch size of 64.

Baselines. NAP [12] is trained on our data on each category individually. CAGE [15] requires an object part graph as input, so we extracted the graph conditions from our dataset and retrained CAGE with our data for all comparisons.

Class	Method	AID		
		COV \uparrow	MMD \downarrow	1-NNA
Chair	NAP [12]	28.3	3.7	89.5
	CAGE [15]	32.9	3.9	92.6
	MeshArt	43.3	3.6	80.2
Table	NAP [12]	21.1	3.0	92.3
	CAGE [15]	25.9	3.9	88.4
	MeshArt	40.2	2.3	71.8
Storage Furniture	NAP [12]	30.6	2.6	85.9
	CAGE [15]	33.4	4.7	80.3
	MeshArt	39.1	2.1	77.1

Table 2. Quantitative evaluation on articulated *structure* generation. MMD values are multiplied by 10^3 . We outperform baselines in all 3 categories in structure generation diversity and realism.

5.1. Evaluation Metrics.

Shape Quality. Evaluating the unconditional synthesis of articulated 3D shapes presents challenges due to the lack of direct ground-truth correspondence; several evaluation metrics have been proposed to compare the distribution of generated and ground-truth objects. We follow prior work [12, 15], and evaluate Instantiation Distance (ID) and Abstract Instantiation Distance (AID). ID evaluates the articulated mesh geometry at different articulation states, while AID evaluates only the object structure at these states. Following [15], we synchronize the articulation states of both generated and ground-truth meshes, using 10 evenly spaced articulation states between the start and end positions. We sample 2,048 points on the surface of the generated mesh or its structure bounding box for ID and AID, respectively. We then compute Minimum Matching Distance (MMD), Coverage (COV), and 1-Nearest-Neighbor Accuracy (1-NNA). Lower MMD indicates better mesh quality, higher COV reflects broader coverage of the real data distribution; for 1-NNA, 50% is optimal.

Perceptual Quality. The aforementioned metrics measure geometric shape quality, but do not address the visual similarity of the generated meshes to the real distribution. To assess this, we render both generated and ground-truth meshes at the same articulation state from eight different viewpoints using Blender, applying a metallic material to emphasize detailed geometric structures. Subsequently, we calculate FID (Fréchet Inception Distance) and KID (Kernel Inception Distance) scores for these image sets. For both FID and KID, lower scores indicate better performance.

5.2. Results

Structure Generation Quality. We evaluate how well our structure transformer covers the articulation structure distribution by unconditionally sampling our model and generating structures at least the same number as the train

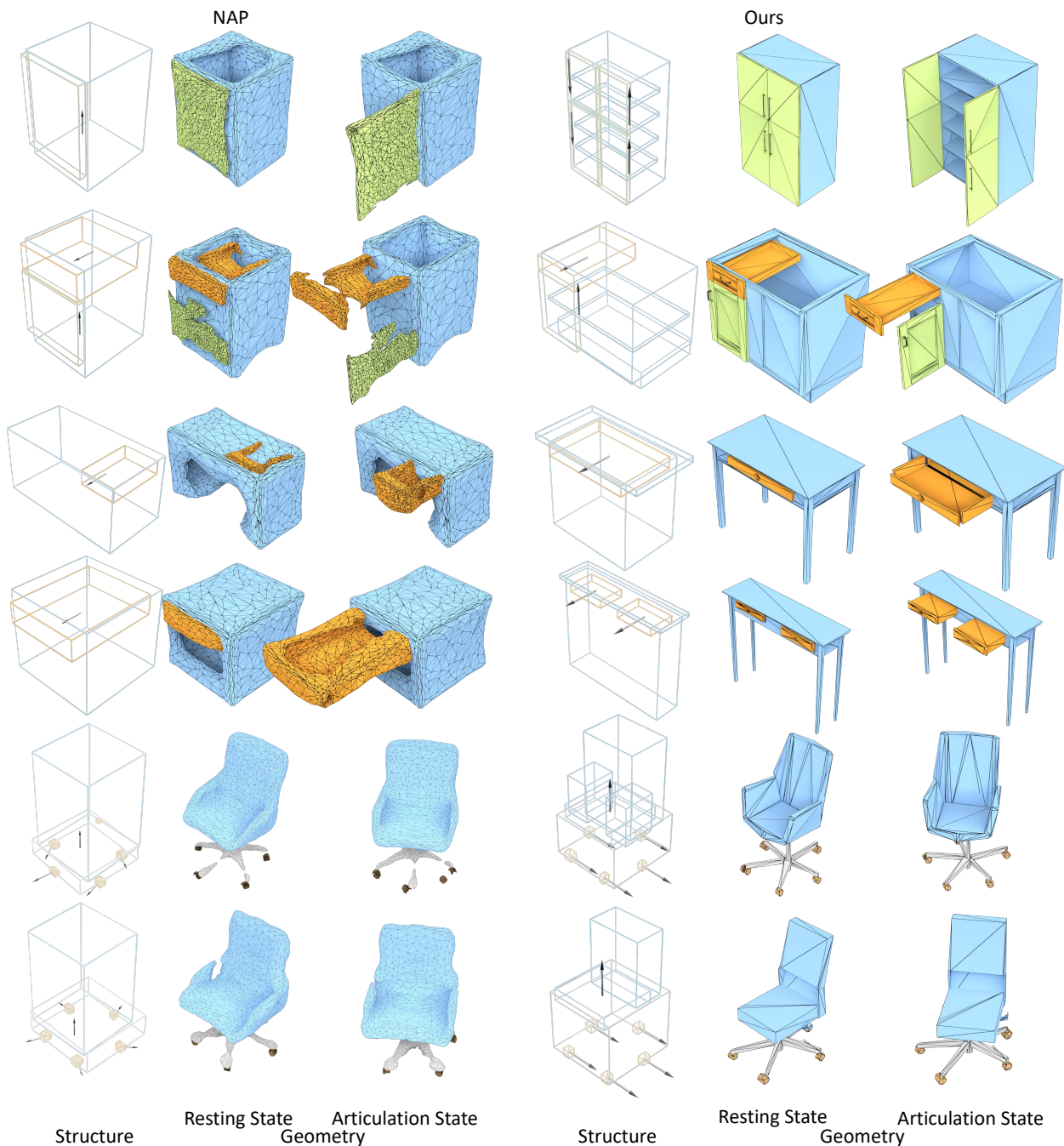


Figure 4. Qualitative comparison across all three categories in our dataset, showing the generated structure with joints, the mesh geometry in its resting state, and an articulated state. Our approach produces compact meshes with sharp geometry, and precise joint generation enables more realistic part movements.

set. Using the generated joint information, we transform these structures across various articulation states and evaluate their AID scores, with results reported in Tab. 2. As shown, our method consistently outperforms both baselines across all three categories.

NAP generates articulation trees where nodes store part geometry information and edges capture relative transfor-

mations and joint information using Plücker coordinates. It needs a post-processing step to extract a valid articulation tree and suffers from modeling intricate articulations, such as the joints are incorrectly predicted for the complex office chairs shown in the last 2 rows of Fig. 4. CAGE requires a category label and a connectivity graph as conditions to produce articulation abstractions. However, CAGE’s generated

Class	Method	ID				
		COV \uparrow	MMD \downarrow	1-NNA	FID \downarrow	KID \downarrow
Chair	NAP [12]	37.1	5.4	88.9	267.7	0.263
	MeshArt	44.0	4.2	73.2	40.8	0.008
Table	NAP [12]	27.9	6.7	89.0	252.6	0.238
	MeshArt	36.9	4.6	78.6	14.3	0.002
Storage	NAP [12]	33.3	4.0	94.1	170.6	0.167
Furniture	MeshArt	41.2	3.1	83.3	8.1	0.002

Table 3. Quantitative evaluation on articulated *mesh* generation. MMD values are multiplied by 10^3 . Our approach outperforms baselines in both shape and visual quality metrics.

structures exhibit repetitive patterns, resulting in lower coverage scores. Our method achieves lower MMD and higher COV scores, demonstrating its ability to produce more realistic and diverse articulation structures.

Articulated Mesh Generation. A key objective of our work is to generate articulated meshes with clean, sharp geometry. As demonstrated in Fig. 4 and Tab. 3, our method consistently outperforms NAP [12] in ID score and visual quality. NAP requires Marching Cubes [17] to decode the final geometry from generated shape codes, resulting in over-smoothed and over-tessellated meshes. In contrast, our approach produces sharper and more compact meshes, effectively preserving sharp geometry details.

Shape Novelty Analysis. We conduct an analysis of our generated shape novelty following [28, 33]. A total of 1000 shapes are generated, and their nearest neighbors in the training set are retrieved based on Chamfer Distance (CD). As shown in Fig. 5, the nearest neighbor analysis demonstrates that our method not only well-captures the training shape distribution (evidenced by low CD values), but moreover, effectively generates novel and realistic shapes (indicated by higher CD values).

5.3. Ablations

Are triangles a better representation for object structures? We consider using the bounding box vertices or the min/max corners as structure parameterizations, encoded with PointNet [24]. As shown in Tab. 4, our triangle parameterization significantly outperforms the baselines, enabling more diverse and realistic articulated structure generation.

Effectiveness of junction face conditioning. Tab. 5 and Fig. 6 shows the effect of our junction face conditioning, in comparison to conditioning only on shape structure information. This notably improves shape consistency and results in more plausible synthesis.

Effect of shape structure conditioning. Fig. 6 and Tab. 5 show that full shape structure conditioning enables more coherent shape generation, thus improving performance.

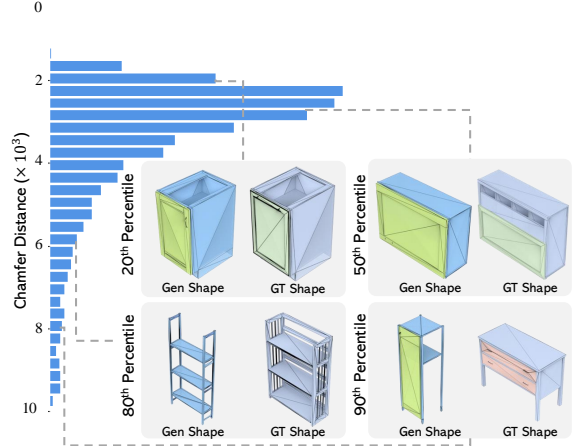


Figure 5. Shape novelty analysis for storage category. We generate 1000 shapes with our method and plot the distribution of their distance to the training set. We visualize the generated shape (left) and its closest train shape (right) at different distance percentiles. The generated shape at the 50th percentile already differs from the closest train shape. This novelty analysis shows that our method can both cover shape distribution (low CD) and generate novel shapes (high CD).

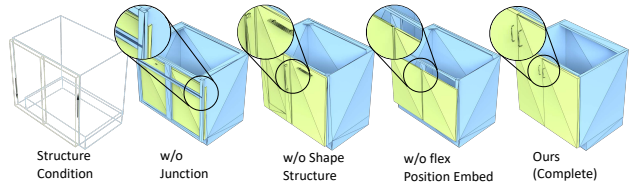


Figure 6. Ablation visualization. Omitting junction guidance (w/o junction) results in part incoherence, while excluding global structure awareness (w/o Shape Structure) produces coherent shapes but lacks style consistency across parts. Without the flexible embedding scheme, the model tends to generate simpler shapes.

Effect of Flexible Embedding. Without the flexible positional embedding, variation in the condition sequence length leads to inconsistent positional embedding features for the mesh part starting token. This inconsistency hinders learning of long-range dependencies, resulting in generating simpler shapes, as illustrated in Fig. 6.

Limitations. While MeshArt shows strong potential in 3D articulated mesh generation, some limitations remain. Our

Method	AID		
	COV \uparrow	MMD \downarrow	1-NNA
Min/Max Bounds	36.3	4.6	84.0
Bbox Corners	35.0	4.4	85.7
MeshArt	39.1	2.1	77.1

Table 4. Ablation study on structure parameterizations (storage category). Using triangles as parameterization notably improves structure generation quality compared to baselines.

Method	COV \uparrow	MMD \downarrow	1-NNA	FID \downarrow	KID \downarrow
w/o Junction Condition	39.1	2.5	80.0	16.7	0.006
w/o Shape Structure Guidance	39.7	2.1	79.7	9.6	0.004
w/o Flex Positional Embedding	40.2	2.1	79.5	8.8	0.003
MeshArt	40.9	2.0	78.7	8.6	0.003

Table 5. Ablation study (storage category). Incorporating structure, local vicinity junctions, and a flexible positional embedding enables our model to generate more diverse and realistic shapes.

transformer-based approach predicts codebook indices for structure and geometry, without full awareness of the decoded surface or articulation motion, making it challenging to enforce physical plausibility, as the codebook selection is non-differentiable. Additionally, while our Articulated PartNet annotations significantly expand training data, its size remains limited for large-scale training. Nevertheless, we see this dataset as a valuable step toward enabling compact articulated 3D mesh generation.

6. Conclusion

We introduced MeshArt, a triangle-based, cohesive hierarchical approach for generating articulated 3D meshes. We decompose objects into coarse part-based structures and detailed part mesh geometries, grounding articulations at the structure level. This enables synthesizing clean, coherent articulated meshes, ensuring both geometric quality and functional properties. We believe MeshArt will drive progress in 3D vision and embodied AI, opening new possibilities for digital agents to learn and interact with the physical world.

Acknowledgements. This project is funded by the Bavarian State Ministry of Science and the Arts and coordinated by the Bavarian Research Institute for Digital Transformation (bidt), the ERC Starting Grant SpatialSem (101076253), and the German Research Foundation (DFG) Grant “Learning How to Interact with Scenes through Part-Based Understanding”. We thank Quan Meng, Yueh-Cheng Liu, and Haoxuan Li for the constructive discussions. We also thank Yueh-Cheng Liu for helping with the supplemental video.

References

[1] Antonio Alliegro, Yawar Siddiqui, Tatiana Tommasi, and Matthias Nießner. Polydiff: Generating 3d polygonal meshes with diffusion models. *arXiv preprint arXiv:2312.11417*, 2023. 2

[2] Yen-Chi Cheng, Hsin-Ying Lee, Sergey Tulyakov, Alexander G Schwing, and Liang-Yan Gui. Sdfusion: Multimodal 3d shape completion, reconstruction, and generation. In *Proceedings of the IEEE/CVF Conference on Computer Vision and Pattern Recognition*, pages 4456–4465, 2023. 1

[3] Angela Dai and Matthias Nießner. Scan2mesh: From un-

structured range scans to 3d meshes. In *Proceedings of the IEEE/CVF Conference on Computer Vision and Pattern Recognition*, pages 5574–5583, 2019. 2

[4] Ziya Erkoç, Fangchang Ma, Qi Shan, Matthias Nießner, and Angela Dai. Hyperdiffusion: Generating implicit neural fields with weight-space diffusion. In *Proceedings of the IEEE/CVF international conference on computer vision*, pages 14300–14310, 2023. 1

[5] Lin Gao, Jie Yang, Tong Wu, Yu-Jie Yuan, Hongbo Fu, Yu-Kun Lai, and Hao Zhang. Sdm-net: Deep generative network for structured deformable mesh. *ACM Transactions on Graphics (TOG)*, 38(6):1–15, 2019. 2

[6] Haoran Geng, Helin Xu, Chengyang Zhao, Chao Xu, Li Yi, Siyuan Huang, and He Wang. Gapartnet: Cross-category domain-generalizable object perception and manipulation via generalizable and actionable parts. In *Proceedings of the IEEE/CVF Conference on Computer Vision and Pattern Recognition*, pages 7081–7091, 2023. 2

[7] Will Hamilton, Zhitao Ying, and Jure Leskovec. Inductive representation learning on large graphs. *Advances in neural information processing systems*, 30, 2017. 4, 1

[8] Kaiming He, Xiangyu Zhang, Shaoqing Ren, and Jian Sun. Deep residual learning for image recognition. In *Proceedings of the IEEE conference on computer vision and pattern recognition*, pages 770–778, 2016. 4

[9] Nick Heppert, Muhammad Zubair Irshad, Sergey Zakharov, Katherine Liu, Rares Andrei Ambrus, Jeannette Bohg, Abhinav Valada, and Thomas Kollar. CARTO: Category and Joint Agnostic Reconstruction of ARTiculated Objects. In *Proc. IEEE Conf. Comput. Vis. Pattern Recog.*, pages 21201–21210, 2023. 3

[10] Zhenyu Jiang, Cheng-Chun Hsu, and Yuke Zhu. Ditto: Building Digital Twins of Articulated Objects from Interaction. In *CVPR*, pages 5606–5616, 2022. 3

[11] Diederik P Kingma and Jimmy Ba. Adam: A method for stochastic optimization. *arXiv preprint arXiv:1412.6980*, 2014. 6

[12] Jiahui Lei, Congyue Deng, William B Shen, Leonidas J Guibas, and Kostas Daniilidis. Nap: Neural 3d articulated object prior. *Advances in Neural Information Processing Systems*, 36:31878–31894, 2023. 3, 5, 6, 8, 2

[13] Jun Li, Kai Xu, Siddhartha Chaudhuri, Ersin Yumer, Hao Zhang, and Leonidas Guibas. Grass: Generative recursive autoencoders for shape structures. *ACM Transactions on Graphics (TOG)*, 36(4):1–14, 2017. 2

[14] Jiayi Liu, Ali Mahdavi-Amiri, and Manolis Savva. Paris: Part-level reconstruction and motion analysis for articulated objects. In *Proceedings of the IEEE/CVF International Conference on Computer Vision*, pages 352–363, 2023. 3

[15] Jiayi Liu, Hou In Ivan Tam, Ali Mahdavi-Amiri, and Manolis Savva. Cage: Controllable articulation generation. In *Proceedings of the IEEE/CVF Conference on Computer Vision and Pattern Recognition*, pages 17880–17889, 2024. 3, 5, 6

[16] Shaowei Liu, Saurabh Gupta, and Shenlong Wang. Building rearticulable models for arbitrary 3d objects from 4d point clouds. In *Proceedings of the IEEE/CVF Conference on Computer Vision and Pattern Recognition*, pages 21138–21147, 2023. 3

- [17] William E Lorensen and Harvey E Cline. Marching cubes: A high resolution 3d surface construction algorithm. In *Seminal graphics: pioneering efforts that shaped the field*, pages 347–353. 1998. 8
- [18] Julieta Martinez, Holger H Hoos, and James J Little. Stacked quantizers for compositional vector compression. *arXiv preprint arXiv:1411.2173*, 2014. 4
- [19] Quan Meng, Lei Li, Matthias Nießner, and Angela Dai. Lt3sd: Latent trees for 3d scene diffusion. *arXiv preprint arXiv:2409.08215*, 2024. 1
- [20] Kaichun Mo, Paul Guerrero, Li Yi, Hao Su, Peter Wonka, Niloy Mitra, and Leonidas J Guibas. Structurenet: Hierarchical graph networks for 3d shape generation. *arXiv preprint arXiv:1908.00575*, 2019. 2
- [21] Kaichun Mo, Shilin Zhu, Angel X Chang, Li Yi, Subarna Tripathi, Leonidas J Guibas, and Hao Su. Partnet: A large-scale benchmark for fine-grained and hierarchical part-level 3d object understanding. In *Proceedings of the IEEE/CVF conference on computer vision and pattern recognition*, pages 909–918, 2019. 2, 5, 6, 1
- [22] Charlie Nash, Yaroslav Ganin, SM Ali Eslami, and Peter Battaglia. Polygen: An autoregressive generative model of 3d meshes. In *International conference on machine learning*, pages 7220–7229. PMLR, 2020. 2, 4
- [23] Adam Paszke, Sam Gross, Francisco Massa, Adam Lerer, James Bradbury, Gregory Chanan, Trevor Killeen, Zeming Lin, Natalia Gimelshein, Luca Antiga, Alban Desmaison, Andreas Kopf, Edward Yang, Zachary DeVito, Martin Raison, Alykhan Tejani, Sasank Chilamkurthy, Benoit Steiner, Lu Fang, Junjie Bai, and Soumith Chintala. Pytorch: An imperative style, high-performance deep learning library. In *Advances in Neural Information Processing Systems 32*, pages 8024–8035. Curran Associates, Inc., 2019. 6
- [24] Charles R Qi, Hao Su, Kaichun Mo, and Leonidas J Guibas. Pointnet: Deep learning on point sets for 3d classification and segmentation. In *Proceedings of the IEEE conference on computer vision and pattern recognition*, pages 652–660, 2017. 8
- [25] Alec Radford, Jong Wook Kim, Chris Hallacy, Aditya Ramesh, Gabriel Goh, Sandhini Agarwal, Girish Sastry, Amanda Askell, Pamela Mishkin, Jack Clark, et al. Learning transferable visual models from natural language supervision. In *International conference on machine learning*, pages 8748–8763. PMLR, 2021. 4
- [26] Barbara Roessle, Norman Müller, Lorenzo Porzi, Samuel Rota Bulò, Peter Kotschieder, Angela Dai, and Matthias Nießner. L3dg: Latent 3d gaussian diffusion. In *SIGGRAPH Asia 2024 Conference Papers*, 2024. 1
- [27] J Ryan Shue, Eric Ryan Chan, Ryan Po, Zachary Ankner, Jiajun Wu, and Gordon Wetzstein. 3d neural field generation using triplane diffusion. In *Proceedings of the IEEE/CVF Conference on Computer Vision and Pattern Recognition*, pages 20875–20886, 2023. 1
- [28] Yawar Siddiqui, Antonio Alliegro, Alexey Artemov, Tatiana Tommasi, Daniele Sirigatti, Vladislav Rosov, Angela Dai, and Matthias Nießner. Meshgpt: Generating triangle meshes with decoder-only transformers. In *Proceedings of the IEEE/CVF Conference on Computer Vision and Pattern Recognition*, pages 19615–19625, 2024. 2, 4, 6, 8
- [29] Yawar Siddiqui, Tom Monnier, Filippos Kokkinos, Mahendra Kariya, Yanir Kleiman, Emilien Garreau, Oran Gafni, Natalia Neverova, Andrea Vedaldi, Roman Shapovalov, and David Novotny. Meta 3d assetgen: Text-to-mesh generation with high-quality geometry, texture, and pbr materials. *arXiv*, 2024. 1
- [30] Minhyuk Sung, Hao Su, Vladimir G Kim, Siddhartha Chaudhuri, and Leonidas Guibas. Complementme: Weakly-supervised component suggestions for 3d modeling. *ACM Transactions on Graphics (TOG)*, 36(6):1–12, 2017. 3
- [31] Aaron Van Den Oord, Oriol Vinyals, et al. Neural discrete representation learning. *Advances in neural information processing systems*, 30, 2017. 4
- [32] Yanzhen Wang, Kai Xu, Jun Li, Hao Zhang, Ariel Shamir, Ligang Liu, Zhiqun Cheng, and Yueshan Xiong. Symmetry hierarchy of man-made objects. In *Computer graphics forum*, pages 287–296. Wiley Online Library, 2011. 2
- [33] Haohan Weng, Yikai Wang, Tong Zhang, CL Chen, and Jun Zhu. Pivotmesh: Generic 3d mesh generation via pivot vertices guidance. *arXiv preprint arXiv:2405.16890*, 2024. 2, 8
- [34] Yijia Weng, Bowen Wen, Jonathan Tremblay, Valts Blukis, Dieter Fox, Leonidas Guibas, and Stan Birchfield. Neural implicit representation for building digital twins of unknown articulated objects. In *Proceedings of the IEEE/CVF Conference on Computer Vision and Pattern Recognition*, pages 3141–3150, 2024. 3
- [35] Rundi Wu, Yixin Zhuang, Kai Xu, Hao Zhang, and Baoquan Chen. Pq-net: A generative part seq2seq network for 3d shapes. In *Proceedings of the IEEE/CVF Conference on Computer Vision and Pattern Recognition*, pages 829–838, 2020. 3
- [36] Zhijie Wu, Xiang Wang, Di Lin, Dani Lischinski, Daniel Cohen-Or, and Hui Huang. Sagnet: Structure-aware generative network for 3d-shape modeling. *ACM Transactions on Graphics (TOG)*, 38(4):1–14, 2019. 2
- [37] Zhenan Wu, Yang Li, Han Yan, Taizhang Shang, Weixuan Sun, Senbo Wang, Ruikai Cui, Weizhe Liu, Hiroyuki Sato, Hongdong Li, et al. Blockfusion: Expandable 3d scene generation using latent tri-plane extrapolation. *ACM Transactions on Graphics (TOG)*, 43(4):1–17, 2024. 1
- [38] Fanbo Xiang, Yuzhe Qin, Kaichun Mo, Yikuan Xia, Hao Zhu, Fangchen Liu, Minghua Liu, Hanxiao Jiang, Yifu Yuan, He Wang, et al. Sapien: A simulated part-based interactive environment. In *Proceedings of the IEEE/CVF conference on computer vision and pattern recognition*, pages 11097–11107, 2020. 2, 5, 6, 1
- [39] Jie Yang, Kaichun Mo, Yu-Kun Lai, Leonidas J Guibas, and Lin Gao. Dsm-net: Disentangled structured mesh net for controllable generation of fine geometry. *arXiv preprint arXiv:2008.05440*, 2(3), 2020. 2
- [40] Linqi Zhou, Yilun Du, and Jiajun Wu. 3d shape generation and completion through point-voxel diffusion. In *Proceedings of the IEEE/CVF International Conference on Computer Vision*, pages 5826–5835, 2021. 1

- [41] Chuhan Zou, Ersin Yumer, Jimei Yang, Duygu Ceylan, and Derek Hoiem. 3d-prnn: Generating shape primitives with recurrent neural networks. In *Proceedings of the IEEE International Conference on Computer Vision*, pages 900–909, 2017. 3

MeshArt: Generating Articulated Meshes with Structure-guided Transformers

Supplementary Material

In this supplementary document, we provide additional details about MeshArt. In Sec. 7, we give more implementation details of our method and loss functions. We elaborate our data annotation process in Sec. 8. We also include additional quantitative comparisons in Sec. 9. We highly encourage readers to watch the supplemental video to see more articulated object generations in action.

7. Method Details

7.1. Structure VQ-VAE

The structure VQ-VAE encodes and quantizes features of bounding box triangles to learn a structured embedding space for articulated object structures. We construct a graph for the triangles by treating each triangle face as a node and connecting neighboring faces with undirected edges. The input node features include positionally encoded triangle coordinates, face area, edge angles, and face normal vectors. These features are concatenated with part semantic, geometry, and articulation attributes projected onto the triangle nodes. The combined features are processed through 4 SAGEConv [7] graph convolutional layers, extracting a feature vector of dimension 768 for each triangle.

At the bottleneck, these embeddings are quantized using a codebook of size 8192, enabling a compact representation of the structure. The decoder reconstructs triangle locations by predicting the logits of discretized coordinates, where both triangle and joint locations are mapped to a uniform grid of size 128^3 .

Instead of directly predicting a discrete part semantic label, the structure VQ-VAE decoder regresses a continuous semantic feature vector from CLIP. The class label is then determined by computing the cosine similarity between the predicted feature vector and the CLIP features of a predefined set of part labels.

The decoder will output a set of joint information per triangle. To obtain a single set of joint predictions per part, the outputs are averaged across all triangles within the part.

This architecture effectively learns quantized embeddings for articulated object structures. These embeddings serve as the basis for the structure transformer, enabling autoregressive generation of object structures with articulations.

Loss Functions. As the triangle coordinates and joint locations are discretized, their reconstruction loss can be formulated as a cross-entropy loss:

$$L_{recon} = \sum_{n=1}^N \sum_{k=1}^{128} \log \mathbf{P}_k, \quad (5)$$

with n being the face index and \mathbf{P}_k representing the predicted probability distribution over the coordinate bins. For part i , its semantic feature \mathbf{l}_i and geometry feature \mathbf{g}_i are supervised using L_2 regression loss:

$$L_{regression} = \|\mathbf{y}_i - \hat{\mathbf{y}}_i\|_2, \quad (6)$$

with y_i, \hat{y}_i being the ground truth and predicted feature vectors.

7.2. Structure Transformer

We use a decoder-only transformer that has a standard GPT-2 architecture, *i.e.*, 12 multi-headed self-attention layers, 12 heads, 768 as feature width, with a context length of 4608. The transformer is trained with cross-entropy loss for next-token index prediction.

7.3. Geometry VQ-VAE

The Geometry VQ-VAE encodes mesh triangle features using an architecture similar to the Structure VQ-VAE. Input triangle features, such as positional encoding, normals, and edge attributes, are processed through 4 SAGEConv [7] layers to extract feature embeddings of dimension 768. These embeddings are quantized at the bottleneck using a vector quantization module with codebook size of 16384, enabling compact and efficient representation.

The 1D-ResNet decoder reconstructs the discretized triangle coordinates by minimizing a cross-entropy loss over a uniform grid. To enforce spatial and structural coherence between parts, the geometry decoder includes an additional channel that predicts the probability of each triangle being a junction triangle, *i.e.*, triangles at the near boundary between adjacent parts. This prediction is supervised with a binary classification loss.

By incorporating junction triangle prediction, the Geometry VQ-VAE not only reconstructs accurate triangle meshes of the target part, but also learns the connectivity information cross parts, supporting smooth articulation and consistent geometry generation.

8. Data Annotation

To effectively learn the distribution of articulated objects, we extend PartNet [21], the largest dataset with object part annotations, by augmenting it with joint information. This augmentation significantly increases the diversity of articulated objects compared to the commonly used PartNet-Mobility [38].

Part Canonicalization. To ensure consistent and meaningful articulation properties, we canonicalize joint anno-

tations. For prismatic joints, all locations are set to the origin of the object’s coordinate system. For revolute joints, we address inconsistencies in part orientations, for instance, chair wheels often have arbitrary orientations in the original dataset, resulting in misaligned revolute joints. To canonicalize these, we rotate each wheel around its vertical axis to align their orientations consistently, as shown in Fig. 7.

Joint Location Generation. For storage furniture and tables, revolute joints are typically located at the “hinge” of an articulated part, often corresponding to one of the four bounding box sides of the part. To automate this process, we generate four hypotheses for joint locations based on the bounding box configuration of the articulated part. An interactive viewer is then used to select the most reasonable joint location, as illustrated in Fig. 8.

Joint Verification. To validate the joint annotations, we render the object at various articulation states and visually inspect the plausibility of the generated motions. This step ensures the accuracy of joint locations and their associated articulation properties, providing high-quality annotations for articulated objects.

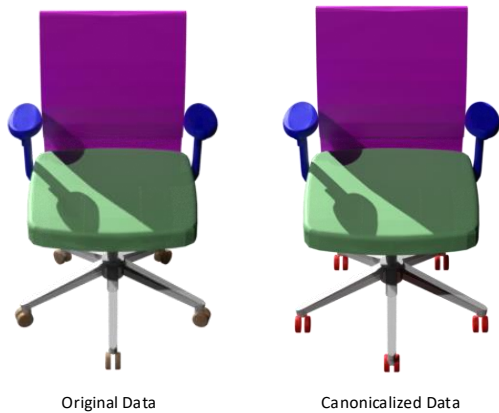


Figure 7. We canonicalize the orientation of different articulated parts for consistent joint annotation.

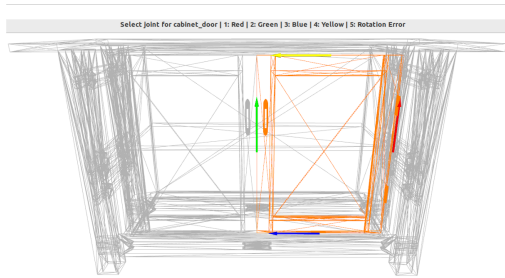


Figure 8. Given a target part, our viewer visualizes the generated joint hypotheses for selection.

Class	Method	COV \uparrow	MMD \downarrow	1-NNA	FID \downarrow	KID \downarrow
Chair	NAP [12]	20.9	5.4	97.3	212.6	0.207
	MeshGPT [28]	34.5	4.2	81.8	24.0	0.011
	MeshArt	27.3	3.8	85.8	23.8	0.013
Table	NAP [12]	20.0	5.8	96.5	243.8	0.231
	MeshGPT [28]	43.0	2.9	69.9	14.5	0.005
	MeshArt	33.4	2.8	77.9	15.1	0.007
Storage Furniture	NAP [12]	25.3	2.9	92.4	162.4	0.142
	MeshGPT [28]	38.7	2.3	81.6	9.3	0.002
	MeshArt	40.9	2.0	78.7	8.6	0.003

Table 6. Quantitative comparison on the task of unconditional mesh generation on a subset of categories from the PartNet [21] dataset. MMD values are multiplied by 10^3 . We evaluate the mesh quality at the resting state for all methods. We outperform the baselines in shape quality, visuals, and compactness metrics.

9. Additional Results

We compare the mesh generation quality of our method with NAP [12], and the state-of-the-art direct mesh generation approach, MeshGPT [28]. Since MeshGPT does not predict object part and articulation information, the evaluation is performed on generated meshes in their canonical resting state. As shown in Tab. 6, we also achieve comparable COV scores to MeshGPT while outperforming the MMD score, indicating higher fidelity in the generated shapes. Notably, our method shows significant mesh generation improvement over NAP on all metrics.